Integrated optimal design for power systems of more electrical aircraft

A. De Andrade, A. Lesage, B. Sareni, T. Meynard, X. Roboam
Université de Toulouse, LAPLACE
UMR CNRS-INPT-UPS
ENSEEIHT, 2 rue Camichel, 31 071 Toulouse, France
e-mail: {name}@laplace.univ-tlse.fr

R. Ruelland, M. Couderc
LIEBHERR AEROSPACE
Avenue des Etats-Unis,
31016 Toulouse, France
e-mail:{mathieu.couderc, regis.ruelland}@liebherr.com

Abstract—**this paper proposes an optimal design approach that aims at coupling a set of design models with an optimization algorithm in order "to improve the integration" of electrical devices and systems embedded in more electrical aircraft. This approach has already been applied to relatively complex power conversion systems like an electrical air conditioning system (ECS) and its interest has been proved. But, elementary components and technologies can also benefit from this approach, and this will be shown on the example of a special magnetic device referred to as Intercell Transformer (ICT).**

Keywords optimal design, design model, power integration, ECS, ICT

I. INTRODUCTION

Among the main trends and future challenges of electrical networks embedded in "more electrical aircraft", mass and loss reduction is of prime importance in terms of competitiveness: "power integration" is then a key factor of this challenge. Optimization of devices and systems integration can be achieved by means of expertise or from classical analysis methods especially based on simulations as it was the case of the MOET EU project between 2006 and 2009. However, novel approaches based on optimization algorithms called "integrated design by optimization" become more and more mature and particularly powerful if subsequent efforts in terms of modeling for design are spent at a system AND component level. Then, "if the 2000s have been the years of network simulation, 2010-2020 could be the decade of Integrated Optimal Design". The Integrated Optimal Design approach consists in coupling sizing models with an optimization algorithm which automatically tunes parameters to optimize system criteria (mass, losses, etc) while satisfying technological and operating constraints (thermal, compliance with quality/stability standards, etc). Weight is certainly the main criterion to be minimized in aircraft systems. However, a tradeoff with losses is classically considered in optimization approaches as minimizing masses leads to reduce sizing then costs of materials which usually increases system losses and related thermal constraints. Thus, minimizing both criteria at the same time indirectly leads to ensure reliability and to increase lifetime of systems.

This paper addresses the issue of optimal design at two distinct levels:

- First, at the system level, the first part concerns the optimal design of an electrical air conditioning system (ECS). Optimization is able to "integrate" major coupling effects between filters, power converter, machine and load in the framework of HVDC network standards and of the flight mission. Such a complex system involves numerous components as, for example, the filtering inductances that can be seen as an elementary design parameter in the optimization process. But, this latter magnetic component may also be seen itself as a more or less complex system, and its design may also be optimized.
- This latter issue is addressed in section III, using a case study of ICTs (Intercell Transformers). As will be shown, this device is already a quite complex system, and optimizing its design to minimize weight is quite

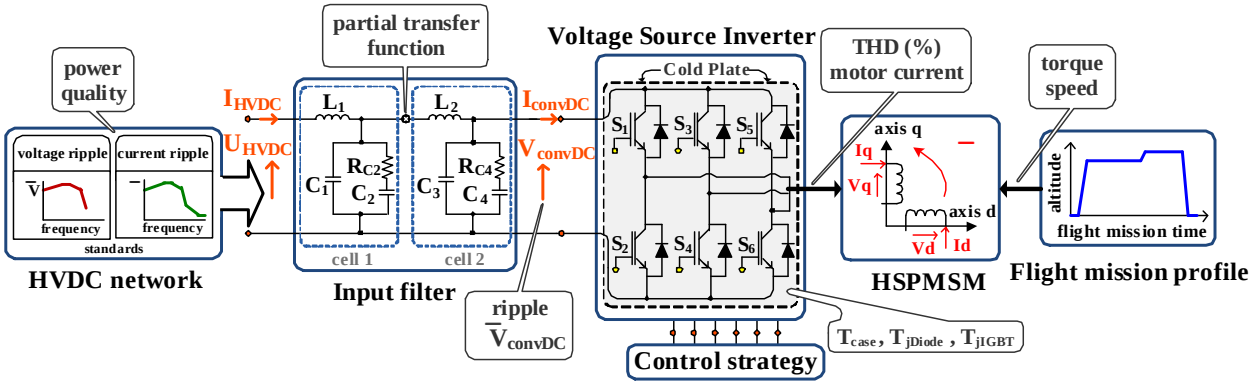

Figure 1. Electrical ECS architecture

challenging. For example, copper losses in this device depend on the combination of leakage inductance and AC resistance, and these parameters are not easy to predict. A dedicated know-how is thus needed to develop a design routine accounting for these phenomena. This quite general approach can also be used to design more standard magnetic components, i.e. inductors and transformers, and the next step will be to merge these design routines for magnetic components with those used for filter design.

II. Integrated Optimal Design of Electrical Environmental Conditioning Systems (ECS)

A. *Introduction*

This first example refers to the integrated design of an electrical ECS system including a High Speed Permanent Magnet Synchronous Machine (HSPMSM) supplied by a PWM Voltage Source Inverter (VSI) associated with an input filter. The cabin conditioning is ensured by the HSPMSM motor-compressor which must operate at specific points in the torque-speed plane depending on the flight mission. On the other hand, the electrical ECS has to comply with HVDC network standards [1] during its operation. Considering the main constraints at the ECS input and output, two design objectives are focused: the whole ECS mass and power losses during the flight mission have to be minimized. In this context, an integrated design process based on the ECS modeling and optimization has been investigated. Our approach particularly emphasizes the importance of taking into account the mission profile in the integrated optimal design process.

B. *Flight mission profile*

HSPMSM operating points that have to be fulfilled in the Torque-Speed plane depend on flight phases (ascent, cruise and descent) and on climatic conditions (i.e., international standard atmosphere, warm or cold weather conditions). These points are illustrated in Fig. 1 with their associated statistic occurrence. It should be noted that the maximum HSPMSM power which approximately corresponds to the maximum speed and maximum torque values is of small occurrence. Setting the HSPMSM base point close to this point would certainly lead to a system oversizing. This underlines the interest of exploiting field weakening and "over-torque" capabilities especially related to thermal capacitances in the integrated design process.

C. *HSPMSM model*

A multiphysics model of the HSPMSM has been derived from a previous PMSM model devoted to ground applications [2], [3]. This model has been extended in order to take all features related to the PMSM behavior at high speed operation (see Fig. 1). It includes:

- all characteristics related to the HSPMSM architecture: material types in each region (iron, magnet, sleeve, copper) and associated geometry parameters (i.e. radius length ratio, slot depth, slot width, number of pole pairs, number of slots per pole per phase, equivalent gap, magnet filling coefficient, etc). This model also allows the computation of the HSPMSM mass from the mass density of each material and from the HSPMSM geometrical features;
- an electric model based on the HSPMSM electrical variables (resistance, leakage and main inductances, magnetic flux, voltage) calculated from the HSPMSM geometrical features;
- a magnetic model specifying HSPMSM electromagnetic behavior in each region (yoke, teethes, air gap, magnet) and magnet demagnetization characteristics;
- the computation of all HSPMSM power losses divided in Joule losses, iron losses [4], aerodynamic losses [5], magnet losses [6];
- a thermal model giving the temperature in each HSPMSM part (copper, insulator, yoke, sleeve, magnet) from the corresponding power losses and from the external temperature imposed by the cooling plate. This model also provides the mass estimation of the HSPMSM cooling system;
- a HSPMSM control strategy allowing maximum torque per Ampere with field weakening mode.

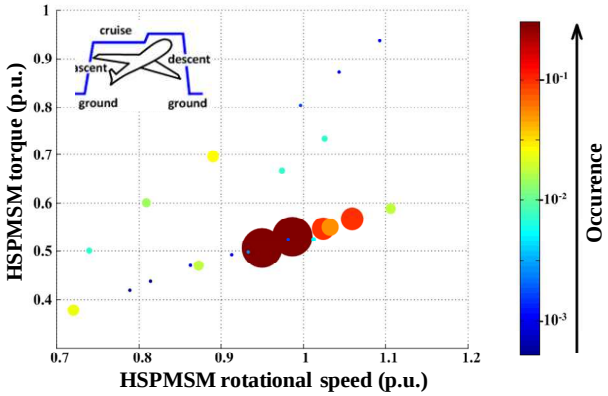

Figure 2. Flight mission in the HSPMSM torque-speed plane

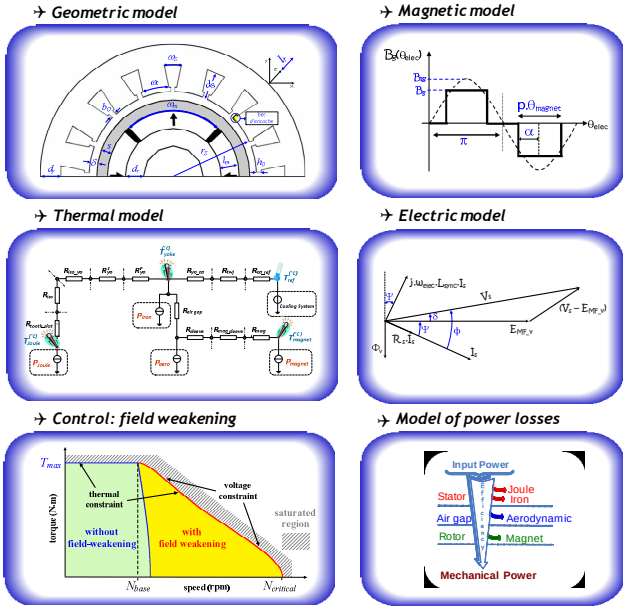

Figure 3. Multiphysics HSPMSM model

D. VSI model

The VSI (Voltage Source Inverter) is a classical 2-level structure (see Fig. 1) associated with a Space Vector Pulse Width Modulation (SVPWM) strategy. The multi-physics VSI model includes:

- a time-frequency approach which allows the determination of the electrical variables (currents and voltages) in time and frequency domains at the VSI input and output. In particular, this approach quickly computes the time evolution of electric variables over a period of the modulation signal at steady state operation. From the SVPWM strategy and the knowledge of VSI switching states, HSPMSM stator voltages are constructed. Then, HSPMSM line currents are easily computed in frequency domain from the HSPMSM impedance using the fast Fourier transform. The corresponding time evolution of HSPMSM currents can also be obtained over the modulation signal period with the inverse fast Fourier transform. Finally, the DC current at the VSI input is deduced from HSPMSM currents and VSI switching states;
- a model of inverter losses including switching losses and conduction losses in diodes and IGBTs;
- a geometrical model depending on the IGBT current rating, the dual pack component features and the cooling plate characteristics. This model gives an estimation of VSI and cooling plate masses;
- a thermal model providing the temperature in each component (diode, IGBT, case) from the associated power losses and from the reference temperature imposed by the cooling plate.

E. Input filter model

The input filter is composed of two cells as depicted in Fig. 1. The corresponding input filter model includes:

- The geometrical and physical features of all filter components. Ferrite inductances are sized according to [7]. Resistance and capacitance elements are extrapolated from WESTCODE [8], AVX [9] and VISHAY [10] manufacturer data;
- a quadripole representation which allows the determination of electric variables at the filter input and output (see Fig. 4. The HVDC input voltage is given by the HVDC standard and the output filter DC current results from the VSI model. Considering those given variables, the other complementary variables (i.e., the input filter HVDC current and the output filter voltage) are found through the quadripole impedance matrix.
- the computation of power losses in the *R*, *L*, *C* filter elements.

F. Electrical ECS optimization

The multilevel ECS optimization has been carried out in [11]. Two different approaches have been compared.

- a local and sequential sizing of each part (i.e. the HSPMSM optimization followed by the VSI and input filter optimization).
- a complete integrated design approach investigating the simultaneous sizing of all coupled components.

1) HSPMSM optimization

The optimal sizing of the HSPMSM has been formulated into an optimization problem with:

- 11 design variables related to the HSPMSM geometric features (number of pole pairs, number of slot per pole per phase, radius length ratio, equivalent gap, magnet filling coefficient) electromagnetic variables (yoke induction, current density) and mechanical characteristics (base speed and base torque);
- 11 constraints associated with geometrical variables (minimum and maximum sleeve thickness, minimum and maximum of copper windings per slots), technological limits (maximum rotational speed, magnet demagnetization) and temperature limits in the different motor parts (magnet, insulator, yoke);
- 2 objectives to be minimized: the HSPMSM mass and the total losses estimated over the flight mission. Total HSPMSM losses are computed by weighting all losses on each mission point according to its occurrence during the flight;

2) VSI and Input Filter optimization

The optimal sizing of the input filter – VSI set has been formulated into an optimization problem with:

- 10 design variables related to the VSI (switching frequency, IGBT current rating) and the *R*, *L*, *C* components of the input filter;
- 11 constraints associated with the input filter features (limitation of the damping coefficient in each branch of the filter, maximum RMS current in the capacitors), with VSI semiconductors (temperature limits in diode and IGBT junctions and in the package case) and with quality standards on the electrical network (quality of low and high frequency currents on the HVDC side, maximum ripple of input VSI voltage, maximum harmonic distortion of the motor current);
- 2 objectives to be minimized: the mass of the input-filter + VSI set and the total losses in this subsystem during the flight mission. The whole losses for this supply part include losses in the filter (*R*, *L*, and *C* losses) and VSI losses (i.e. switching and conduction losses).

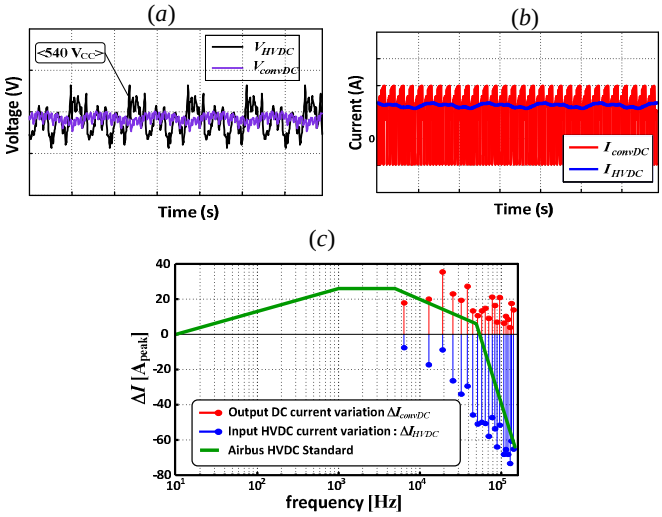

Figure 4. Typical plots of electrical variables at the filter input and output (*a*) Input and output voltages (*b*) Input and output currents (*c*) Input and output current harmonics compared to HVDC standards

3) *Results*

We first perform the sequential ECS optimization by determining HSPMSM Pareto-optimal configurations before optimizing the ECS supply part. Those solutions are obtained from 10 independent runs of the NSGA-II evolutionary algorithm [12] with a population size of 100, and number of generation of 500 and using a self-adaptive recombination [13]. Fig. 5*a* compares the optimal tradeoffs found in the objective space (i.e. HSPMSM mass and losses) with a reference non-optimized solution. All variables are given in per unit (pu) for confidentiality reason. Even if some important gains on both HSPMSM objectives can be observed, we point out that they could not be considered as significant at the ECS system level since the ECS supply part is not designed at this step. Then, the multiobjective optimization of the input filter-VSI set is also performed with regards to three particular HSPMSM configurations extracted from the previous Pareto-optimal front. With respect to the reference HSPMSM solution, those configurations are chosen at the same level of mass (i.e. M1), at the same level of losses (i.e. M2), the "M3" motor being an intermediate dominant solution. Pareto-optimal solutions of input filter – VSI set are obtained as previously from NSGA-II runs considering the three particular HSPMSM configurations. Results are illustrated in Fig. 5*b*. The particular shape of the Pareto-optimal front clearly indicates "a weak front", i.e. the lack of compromise between both objectives. Therefore, only input filter+VSI configurations with minimum mass are considered as optimal solutions.

Finally, the simultaneous multiobjective optimization of all ECS components is investigated in a single optimization loop. In comparison with both component optimization problems described in the previous subsections, the complexity of this "system" problem is significantly increased since all design variables and constraints are aggregated. Therefore, this new problem includes 21 design variables, 22 constraints and 2 objectives. It is then solved using the NSGA-II with a population size of 100 and a number of generations of 1000. Pareto-optimal ECS solutions obtained from this system optimization are illustrated in Fig. 5*c* and compared with the three ECS solutions resulting from the sequential optimization approach (combination by mass and losses additions of HSPMSM and VSI-input filter solutions of Fig. 5*a* and Fig. 5*b*). As expected, the simultaneous optimization of all components clearly outperforms the sequential optimization approach. However, it should be mentioned that convergence on the system optimization problem can be obtained in a reasonable time only if the optimal components found by the sequential approach are inserted in the NSGA-II population.

III. FOCUS ON THE DESIGN OF AN INTERCELL TRANSFORMER

A. *Principle of the InterCell Transformer*

InterCell Transformers (ICTs) are the key components of parallel interleaved converters that allow improving the quality of the waveforms generated at the input *and* output of a macro-commutation cell. Mastering the design of magnetic components in general is essential because they represent a significant part of the weight, cost and complexity of the equipment, and the case of the ICTs is critical because they open the way to higher specific powers. In this section, we describe a design procedure for such a component, taking the example of the topology in Fig. 6. In this topology, the 8 commutation cells are controlled with the same duty cycle but they are phase-shifted by 360°/8 to optimize the input-output waveforms. The ICT has 8 bobbins wound on a monolithic magnetic core and the coupling results in all currents to be equal with a ripple at $8.f_{sw}$.

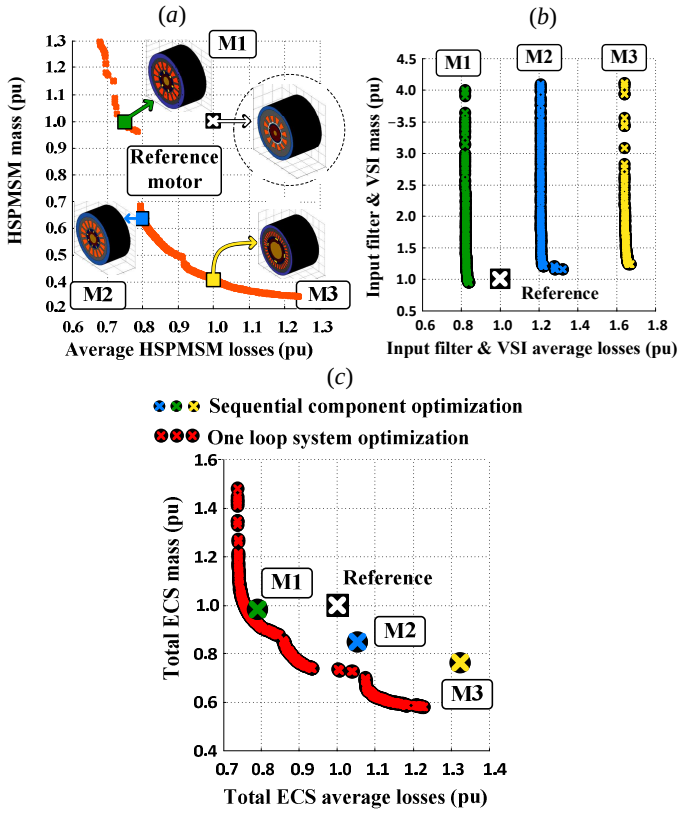

Figure 5. Pareto-optimal ECS configurations
(*a*) HSPMSM optimal configurations (*b*) Input filter & VSI optimal configurations relative to three particular HSPMSM solutions (M1, M2, M3) (*c*) ECS optimal congfigurations obtained from sequential component or system optimization

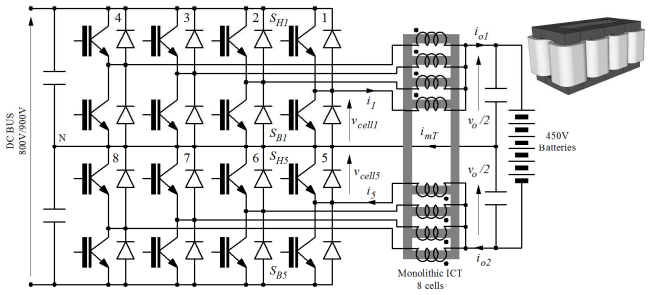

Figure 6. Series-Parallel DC-DC converter with an 8-way ICT

B. *Design*

The design of an ICT basically involves the same steps as the design of other magnetic components:

- determine the current and flux densities based on circuit excitations and geometrical parameters,
- determine loss densities in the different parts, and then total losses by integration over the full volume,
- determine the temperature rise based on a thermal model taking into account the geometry and size of the ICT and the external conditions (temperature natural/forced convection),
- check for compliance with material limit temperatures.

However, in the case of the ICT, these steps involve specific problems that can be summarized as follows:

- the current ripples depend on the leakage flux with a significant part flowing unguided in the air which makes the inductance difficult to evaluate,
- this current ripple can be at a high frequency thus flowing unevenly through the conductors,
- the flux waveforms in some regions of the ICT can significantly differ from the sinusoidal waveforms used to characterize materials, and even the determination of the pk-pk flux is not always trivial; both these reasons make the evaluation of core losses a difficult task.

In the following, we describe how these questions have been addressed to design this component. Simplified models of the different aspects of the design have been developed (interpolated surface response of finite element simulations for leakage inductance and AC resistance, reluctance model for magnetizing fluxes, Forest & Sullivan model for core losses under non sinusoidal induction, extremely basic thermal-resistance-based thermal model) and included in a matlab optimization routine (fmincon, gradient type algorithm, with weight minimization and constrained induction and temperature).

A lot of efforts have been made to make these models accurate, but there are still a number of assumptions to make calculation fast enough for inclusion in an optimization routine. For this reason, at the end of the design it is a good practice to allow more accurate calculation by means of heavier models to check the design before construction of the prototype.

The design of a monolithic ICT such as that in Fig. 7 is, strictly-speaking, a 3D electromagnetic problem, especially when AC resistance and leakage flux are concerned. However, we think it is interesting and possible to develop a design procedure using simpler models. The first step is to identify cutting planes (Fig. 7*a*) that allow studying the *n*-phase ICT device as an assembly of *n* pairs of windings, each pair being studied in 2D (Fig. 7*b*).

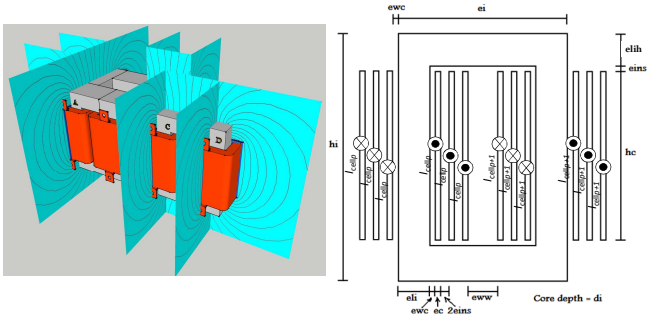

a – Cutting planes b – flat 2D representation

Figure 7. 2D model of the *n*-phase ICT

1) *Winding losses*

The first problem to be solved is the evaluation of the AC resistance of the windings. The model derived by Dowel can be used when the field varies along one dimension only, and this is typically the case inside the windows of the ICTs that we want to design when:

- the window is rectangular,
- the core permeability is very high,
- and the most visible part of the current ripple gives a zero amps-turns product inside the window.

For this reason, a design procedure based on this model has first been developed, but there are a number of phenomena that cannot be accounted for with the Dowel model because they involve a 2D field distribution:

- the AC resistance outside the window,
- the AC resistance inside the window when the core permeability is low,
- the AC resistance corresponding to the magnetizing current.

For these reasons, a routine allowing to vary the size parameters defined in Fig. 7*b*, to launch a Finite Element simulation (FEMM software) for different frequencies and for common currents ($I_{\text{cell}p}=+I_{\text{cell}p+1}$, Fig. 8a), and differential currents ($I_{\text{cell}p}=-I_{\text{cell}p+1}$, Fig. 8*b*).

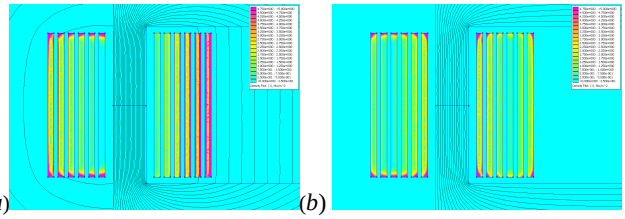

(*a*) (*b*)

Figure 8. FEMM simulation of a simple ICT (Current density plot) (*a*) coupled current (*b*) magnetizing current

Intensive use of this routine allows generating a file containing the four characteristic resistances (AC per-meter-resistance inside and outside the window for both common and differential modes) and the characteristic inductances (leakage per-meter-inductance inside and outside the window) corresponding to a wide range of size parameters. This file is generated off line and later used by the design routine to evaluate AC resistances and leakage inductance by means of interpolation. The total AC copper losses are finally calculated by summing up the contributions of the different currents (DC,

AC common and AC differential) at different frequencies (resp. 0, multiples of n_{Cell}. f_{sw} and multiples of f_{sw}) in the different parts of the ICT (integration of per-meter losses inside and outside the window).

Table I gives an example of the figures obtained through this process for a 2-cell ICT with 6 turns per winding, a switching frequency of 15 kHz. The magnetizing and coupled currents are assumed to be triangular and the 5 first terms of the Fourier series are evaluated for a duty cycle of 25%. The results in this table depend on many factors and cannot be used to justify neglecting one factor or the other; they are shown here only to illustrate the fact that R_{AC} can be significantly higher than R_{DC} and that calculating losses based on DC resistance only can be quite wrong, even at relatively low frequency.

TABLE I. AC/DC RESISTANCE RATIO SIMULATION RESULTS

rank	a_n I_{diff}	R_{acn}/R_{dc} ext-diff	R_{acn}/R_{dc} int-diff	a_n I_{com}	R_{acn}/R_{dc} ext-com	R_{acn}/R_{dc} int-com
1	1	1.64	1.43	1	3.12	2.28
2	0.35	2.12	1.81	0	4.78	5.86
3	0.11	2.58	2.26	0.11	6.58	11.29
4	0	3.07	2.78	0	8.55	17.97
5	0.04	3.58	3.38	0.04	10.60	25.30
$\sum_{n=1}^{5}\frac{R_{ACn}}{R_{DC}}a_n^2$		1.95	1.69		3.21	2.46

2) Core Losses

The monolithic ICT is a forced flux device ; the electrical circuit imposes a square AC voltage across the winding that becomes a triangular flux source of which peak amplitude is easily determined:

$$\hat{\Phi}_{AC}^{\max} = \max\left(\frac{D.(1-D).V}{2n_t.f}\right) = \frac{V}{8n_t.f}$$

These flux sources are connected to a reluctance network that can be modeled as shown in Fig. 9, and they induce fluxes in the linking legs that depend on the control sequence. It has been found that the normal phase sequences generate very high fluxes in linking legs and that modified sequences can reduce these fluxes to 50% of the flux in the windings [14]

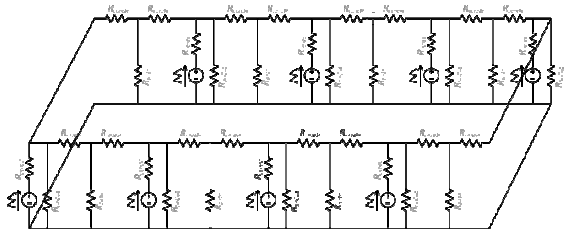

Figure 9. Reluctance model of the *n*-phase ICT

During the optimization process, core losses are evaluated using the peak-peak value of these fluxes a simple Steinmetz model and loss characteristics provided by the manufacturer. In order to enlarge the domain of validity of this model a fitting of losses in various materials has been made in the form of:

$$LossDensity = \left(K_1.f^{\alpha_1} + K_2.f^{\alpha_2}\right)\Delta B^{(\beta - a_\beta.f)}$$

3) Thermal model

To estimate the temperature rise it is assumed that core and winding temperatures are homogenous; their respective exchange surfaces are calculated as a function of the different size and shape parameters and exchange coefficients are defined.

4) Design by optimization

The ICT is defined as a 3D object by means of a set of parameters including independent size parameters and the number of cells. It seems a good practice to use an initial guess satisfying the constraints to help convergence; in our case, that means taking a big ICT as an initial guess. Using the approach described in former paragraphs, core losses, winding losses, weight and temperature rise are computed. A standard gradient routine is used to minimize weight and maintain the temperature at an acceptable value. The current ripple which is often considered as a specification for the design of magnetic is considered as a simple output; in fact, high current ripple tends to increase losses, and optimizing for weight limits naturally this current ripple to an acceptable level. In addition, should filtering be insufficient, it is generally preferred to minimize the magnetic component and increase capacitance.

Geometrical quantities		Electrical quantities	
e_c	0.3663mm	f_{sw}	20 kHz
h_c	66.93mm	R_{dc}	4.618 mΩ
eli	30mm	R_{ac}	344.3 mΩ
eli_h	12.52mm	L_{acNHF}	16.38 µH
di	29mm	L_{mag}	592.1 µH
N_t	15 turns	$P_{condTotal}$	268.2 W
Vol_{Cond}	599969 cm^3		
Vol_{Core}	877899 cm^3	Magnetic quantities	
		B_{dc}	0.1269T
Thermal Quantities		B_{hf}	0.4663T
$\Delta\theta_{Cu}$	45°C	B_{max}	0.360T
$\Delta\theta_{Fe}$	29.92°C	P_{core}	69.26W

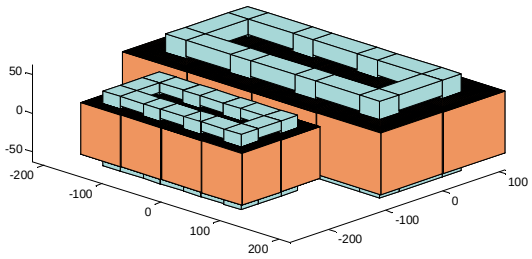

Figure 10. Dimensions of the ICT . Right: initial guess, Left: optimized

5) Final check

After optimization converged, several checks can be made: AC resistance and leakage inductances are calculated via finite elements to improve the estimation made by interpolation. Copper losses of the final solution can be recalculated and compared to the initial estimate.

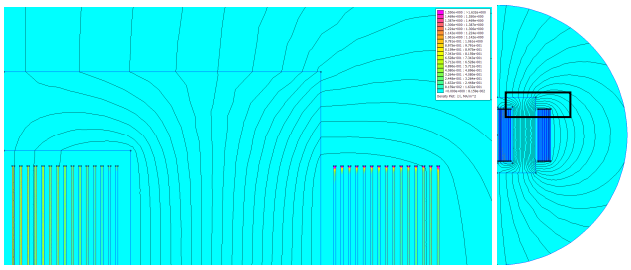

Figure 11. Finite element analysis of the optimized ICT

The values extracted from this simulation are: R_{ac}=272mΩ; L_{ac}=23 µH; P_{condLF}=33 W; $P_{condNHF}$=0.25 W; $P_{condTotal}$=265 W

In this case, the conduction losses induced by the current ripple at $n_{Cell}.f_{sw}$ are very low (0.25 W per phase compared with 33 W per phase for DC-induced losses); as a consequence, the decrease in R_{ac} (272 mΩ by FEMM instead of 344 mΩ by interpolation) and the increase of L_{ac} (24 µH in FEMM instead of 16 µH with the interpolation) only result in a very slight decrease of the total conduction losses. Core losses are also re-calculated; knowing the number of cells and having a better estimate of the different reluctances, it is possible to determine the fluxes and the induction in all branches of the core. The iGSE [15] is then applied to these complicated waveforms to estimate the extra losses induced by the *dB/dt* that is significantly higher than that of a triangular waveform with the same *pk-pk* amplitude. In this design, we find that the maximum *pk-pk* induction (obtained at 50% duty cycle) is 0.37 T in the windings and 0.44 T in the linking legs, but it is mainly the higher *dB/dt* observed in linking legs that generates a higher loss density (95 kW/m^3 in the linking legs vs 60 kW/m^3 in the winding legs).

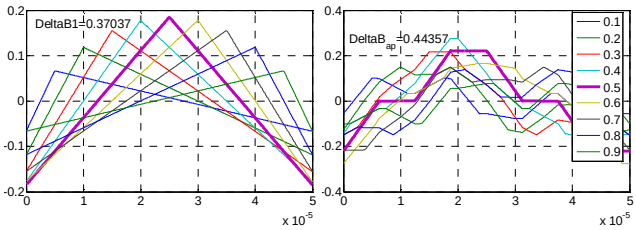

Figure 12. Induction vs time for different duty cycles
left: winding legs, right: linking legs

For the present application, thermal issues were considered to be critical, and once the geometry of the ICT was found, thermo-fluidic simulations have been performed with IcePak to re-evaluate the values assigned to exchange coefficients. We imposed an air flux with a speed of 5m/s and a temperature of 55°C, and the core and winding loss densities determined previously were imposed as heat sources. The average temperature in the conductors settled around 100°C and the one in the core around 77°C. Using the exchange surfaces calculated with our tool, exchange coefficients of 37 W/K/m² and 42 W/K/m² were respectively found for the windings and for the core. Surprisingly enough, the initial estimate of 36 W/K/m² turned out to be a very good estimate, at least for the windings. The exchange coefficient for the core is not as good, but the core temperature seemed to be still on the safe side so we decided to stick to this design. It should be noted that the first guess on the exchange coefficient is not always as good and in general a full design process needs at least a second iteration by rerunning the optimization with a value of the exchange coefficient that has been defined for an object with a shape and size that is close to those of the final object.

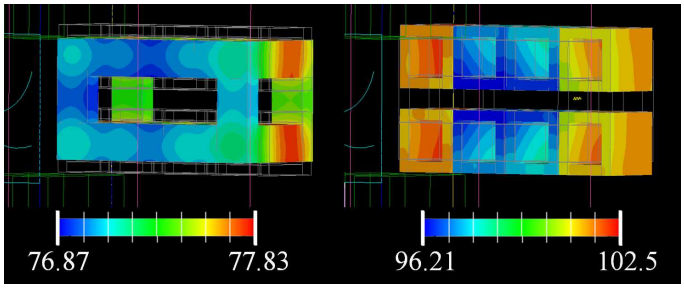

Figure 13. ICT infrared image for nominal operating point

C. *Building the prototype*

Finally the prototype was built using custom made core with the right shape and size (Fig. 14).

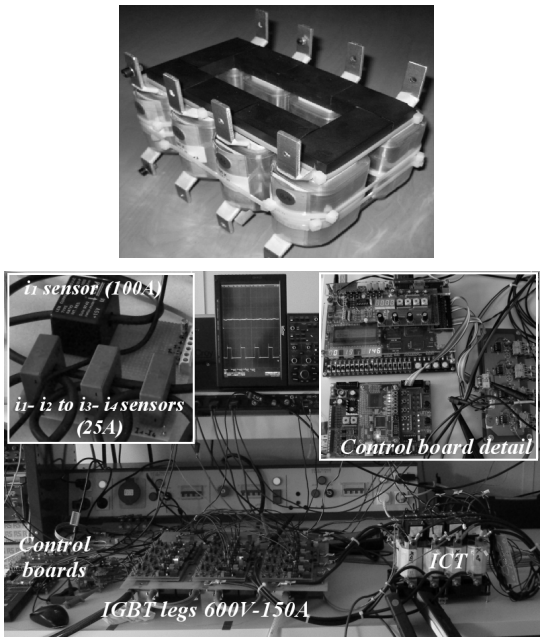

Figure 14. Experimental setup – top: ICT; bottom: Converter and control & instrumentation

Generic inverter legs have been used to test the ICT in an opposition configuration to avoid handling high power and to allow accurate efficiency measurements.

D. *Experimental results*

The device has been tested up to 800 V on the DC bus and 90 A per phase which for D=50% gives 400 V/360 A on the low voltage side and a power of 144 kW.
Thermal tests have also been done at 600 V/360 A (because the legs we used cannot operate at full power for a long time). As can be seen from Fig. 16, the maximum steady state

temperature of the winding is around 65°C with a room temperature of 25°C (100°C estimated for 800 V/90 A with room temperature of 55°C). The main difference between these two points of operation is an increase of core losses, which will mainly affect core losses and this will be checked in coming months.

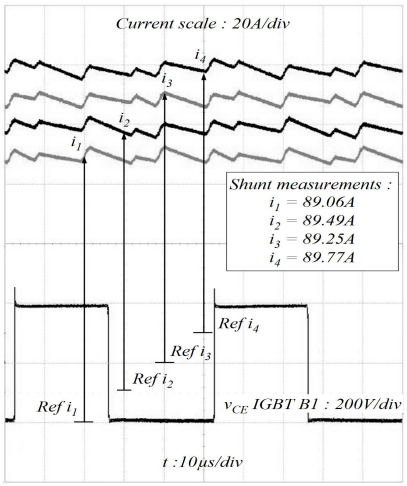

Figure 15. Waveforms at nominal operating point

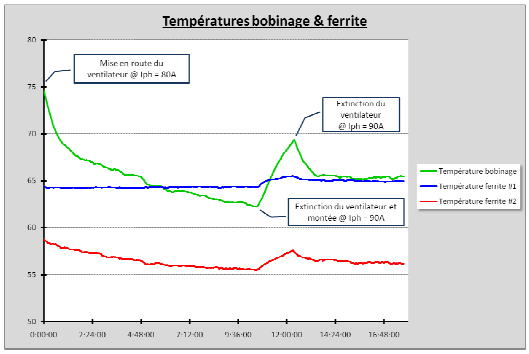

Figure 16. Waveforms at nominal operating point

The design process presented here has been applied to other magnetic components, including an isolated ICT combining three functions ; inter cell coupling, current smoothing and primary-secondary insulation [17]. Such a device could be used for a typical aeronautics application: 10 kW 28/270 V conversion.

IV. Conclusion

Two complementary level of mass and losses optimization have been focused in this paper. The first one concerns a whole ECS. Two optimization approaches have been proposed: a sequential approach with two optimization loops separating power supply and actuation parts. Then, a global optimization with a unique loop integrating all couplings between HVDC network and actuation application with respect to the flight mission has been presented: the simultaneous optimization of all components clearly outperforms the sequential optimization approach.

The second optimization level concerns the design of magnetic components which is not a trivial task, especially when InterCell Transformers are concerned because losses are governed by the leakage inductance and the AC resistance that are difficult to predict. Intensive work on the subject now allows designing such components in a quite accurate way. Designing ICTs for other power levels or other switching frequency, or to optimize weight of onboard systems will be a way to test the limits of application of the design procedure.

Acknowledgment

These studies have been partially achieved in the framework of ISS and PREMEP projects. ISS is funded by the French DGAC (Direction Générale de l'Aviation Civile). PREMEP is funded by the French "Direction Générale des Entreprises", Midi Pyrénées region, Aquitaine Region.

References

[1] Airbus Directives (ABD) and Procedures, ABD0100-Equipment-Design, General Requirements For Suppliers, Issue C, 1998.

[2] B. Sareni, A. Abdelli, X. Roboam, D. H. Tran, "Model simplification and optimization of a passive wind turbine generator", *Renewable Energy*, Vol. 4, n°12, pp2640-2650, 2009.

[3] D. H. Tran, B. Sareni, X. Roboam, C. Espanet, "Integrated Optimal Design of a Passive Wind Turbine System: An Experimental Validation", *IEEE Transactions on Sustainable Energy*, Vol 1, n°1, pp. 48-56, 2010.

[4] C. Mi, G.R. Slemon, R. Bonert, "Modeling of Iron Losses of Permanent-Magnet Synchronous Motors", *IEEE Trans. On Industry Applications*, Vol. 39, n°3, pp. 734-741, 2003.

[5] J.E. Vrancik "Prediction of windage power loss in alternators", Nasa Glenn Research Center, USA, Technical Note D-4849, Octobre 1968

[6] D. Ishak, Z. Q. Zhu, and D. Howe, "Eddy-current loss in the rotor magnets of permanent-magnet brushless machines having a fractional number of slots per pole", *IEEE Trans. Magn.*, vol. 41, n° 9, pp. 2462-2469, 2005.

[7] F. Leplus, "Bobine à noyau de fer en régime variable," Techniques de l'ingénieur D-3040, 2007.

[8] See: http://www.westcode.com/

[9] See: http://www.avx.com/

[10] See: http://www.vishay.com/

[11] A. De Andrade, B. Sareni, X. Roboam, M. Couderc, R. Ruelland, "Multilevel optimization of electrical environemental conditioning systems for more electrical aircrafts", *12th Workshop on Optimization and Inverse Problems in Electromagnetism* (OIPE'12), Ghent, Belgium, 18-21 september 2012.

[12] K.Deb, *Multi-Objective Optimization Using Evolutionary Algorithms*, Willey, 2001.

[13] B. Sareni, J. Regnier, X. Roboam, "Recombination and Self-adaptation in Multiobjective Genetic Algorithms", *Lecture Notes in Computer Science*, Vol. 2936, pp. 115-126, 2004.

[14] T. Meynard, F. Forest, F. Richardeau, E. Labouré," Procédé et dispositif d'alimentation d'un coupleur magnétique ", Demande de brevet PCT/FR2006/001579, 04 Juillet 2006, Demande de brevet Français N° 05 07136, Déposé le 5 juillet 2005

[15] F. Forest, T. Meynard, E. Labouré, V. Costan, A. Cunière, T. Martiré, "Optimization of the Supply Voltage System in Interleaved Converters Using Intercell Transformers", *IEEE Transactions on Power Electronics*, Vol. 22, n° 3, pp. 934-942, May 2007.

[16] K. Venkatachalam, C.R Sullivan, T. Abdallah, H. Tacca, "Accurate prediction of ferrite core loss with nonsinusoidal waveforms using only Steinmetz parameters," *Computers in Power Electronics, 2002. Proceedings. 2002 IEEE Workshop on* , vol., no., pp. 36- 41, 3-4 June 2002.

[17] F. Forest, B. Gelis, J.J. Huselstein, B. Cougo, E. Laboure, T. Meynard, "Design of a 28V-to-300V 12kW MultiCell Interleaved Flyback Converter Using InterCell Transformers", *IEEE Transactions on Power Electronics*, Vol. 25, n° 8, pp 1966-1974, August 2010.